Supporting Information

The Role of Hydrogen in Defining the n-Type Character of $BiVO_4$ Photoanodes

Jason K. Cooper,[a,b] Soren B. Scott, [a] Yichuan Ling,[c] Jinhui Yang,[a,b] Sijie Hao,[d] Yat Li,[c] Francesca M. Toma,[a,b] Martin Stutzmann,[d] K. V. Lakshmi,[e] and Ian D. Sharp[a,b]

[a.] *Joint Center for Artificial Photosynthesis, Lawrence Berkeley National Laboratory, Berkeley, CA 94720, United States*
[b.] *Chemical Sciences Division, Lawrence Berkeley National Laboratory, Berkeley, CA 94720, United States*
[c.] *Department of Chemistry and Biochemistry, University of California, Santa Cruz, CA 95064, United States*
[d.] *Walter Schottky Institut and Physik Department, Technische Universität München, Am Coulombwall 4, 85748 Garching, Germany*
[e.] *Department of Chemistry and Chemical Biology and The Baruch '60 Center for Biochemical Solar Energy Research, Rensselaer Polytechnic Institute, Troy, NY 12180, United States*

1. Scanning electron microscopy (SEM)

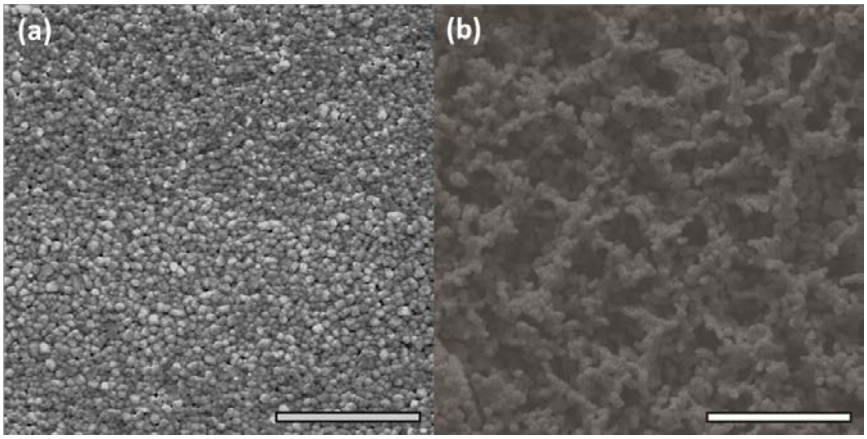

Figure S1. Scanning electron micrographs comparing the morphologies of $BiVO_4$ formed by spin coating (a) and electrodeposition (b). The nanoporous structure of the electrodeposited material results in a higher photocurrent density compared to the planar spin coated material. The scale bar is 2 μm in both images.

2. Frontside vs. backside illuminated photoelectrochemical performance characteristics

J-E curves for both frontside and backside illumination of both the as-grown and 265 °C H_2-annealed samples are co-plotted (same data as Main Text Figure 1a and b), so that the traces may be more easily compared. Backside illumination in the as-grown material produces a significantly larger photocurrent

density compared to frontside illumination. Importantly, the *J-E* curves for the H_2 annealed sample are independent of illumination orientation.

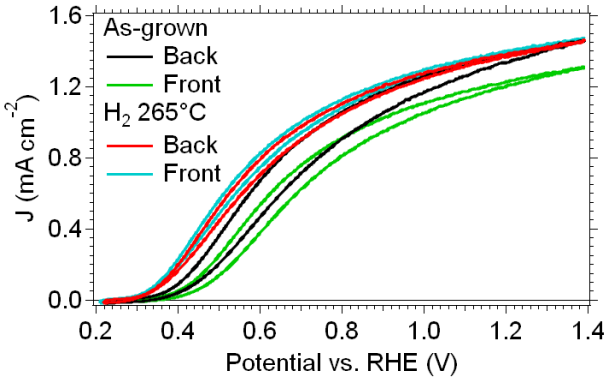

Figure S2. Photoelectrochemical testing, under AM 1.5G 1 Sun illumination and in 1 M phosphate buffer (pH 6.8) with 0.1M Na_2SO_3, of $BiVO_4$ films deposited on FTO, showing the second cycle from open-circuit voltage to 1.4 V vs RHE. As-deposited films are compared to films annealed in hydrogen at 265°C under frontside and backside illumination.

3. X-ray diffraction (XRD)

Figure S3 shows X-ray diffraction (XRD) of thin films grown on FTO (top), powders (middle), and references (bottom). The references for $BiVO_4$, Sn, and V_2H come from the powder diffraction files (PDF) maintained by the International Center for Diffraction Data (ICCD). The reference for FTO is a scan of an FTO substrate before deposition. The XRD patterns for the powders show high-purity monoclinic scheelite $BiVO_4$. There were no observable structural changes to the monoclinic phase as a result of H_2 annealing up to a temperature of 290 °C. The thin films are consistent with polycrystalline $BiVO_4$ films on FTO up to a H_2 annealing temperature of 300 °C. The thin film annealed in H_2 at 320 °C, which turned visibly black as a result of the treatment, shows signs of metallic tin (from the FTO) and perhaps also vanadium hydride (V_2H), consistent with a destructive removal of oxygen and reduction of the material due to annealing at this temperature. This formation of reduced products was also confirmed by XPS (below, Figure S6).

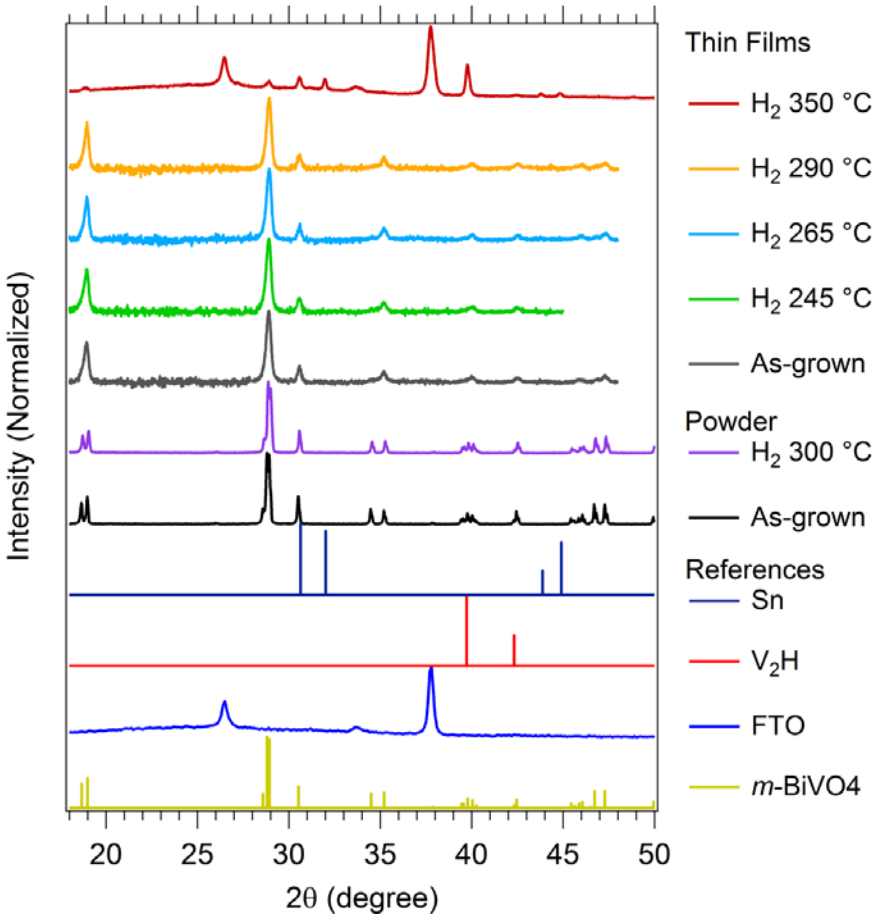

Figure S3. XRD of $BiVO_4$ thin films on FTO, powders, and references (as indicated in figure legend).

4. Raman spectroscopy

Raman spectroscopy of untreated and H_2-annealed samples show no change in vibrational states (Figure S4). There were no observable shifts in the vibrational modes, consistent with the lack of crystalline changes as a result of H_2-annealing up to 290-300 °C.

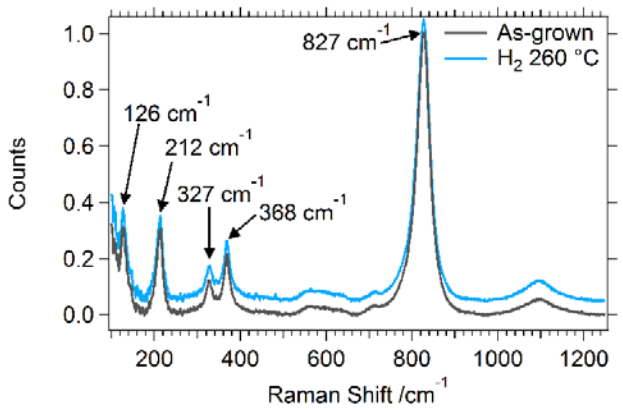

Figure S4. Raman spectra of $BiVO_4$/FTO thin-films: as-grown (black) and annealed in hydrogen at 265 °C (blue). The spectrum from the treated sample is shown with a vertical offset for ease of viewing.

5. Dark electrochemical *J-E* characteristics

Current-voltage plots obtained during cyclic voltammetry without illumination are shown in Figure S5. The untreated and H_2-annealed samples show negligible dark current. The sample annealed at 320 °C shows a very large anodic current in the first cycle, which is consistent with oxidation of metallic species, indicating the sample was reduced at this high annealing temperature.

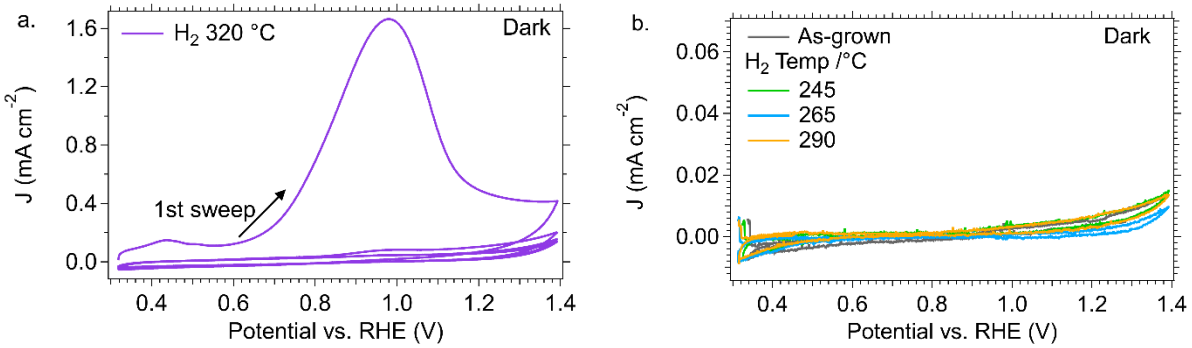

Figure S5. Current density vs. electrochemical potential measured without illumination for as-grown and H_2-treated $BiVO_4$ films spin-coated on FTO with a scan rate of 20 mV/s. (a) First three cycles between E_{OC} and 1.4 V vs. RHE of the 320 °C H_2-annealed sample. (b) Measurements obtained on as-grown and H_2-treated samples.

6. X-ray photoelectron spectroscopy (XPS)

Comparison of XPS spectra of as grown 320 °C H_2-treated $BiVO_4$/FTO films confirmed the presence of reduced species and the removal of oxygen from $BiVO_4$ after annealing at the highest temperature

(Figure S6). The Bi 4f spectrum (Figure S6a) from the 320 °C H_2-treated film shows peaks corresponding to metallic bismuth and an accompanying loss of the peak associated with Bi^{3+} in $BiVO_4$. This magnitude of the Bi 4f signal was reduced by ~10x, indicating that Bi is also removed from the surface. The O 1s signal from the $BiVO_4$ was nearly completely eliminated by H_2-annealing at 320 °C, leaving only signal from the underlying FTO, which became exposed by the process (Figure S6b). The V $2p_{3/2}$ core level signal was correspondingly broadened to lower binding energy, indicating significant reduction of oxidation state (Figure S6c). Finally, the valence band spectrum following this annealing treatment exhibited none of the features characteristic of $BiVO_4$ features and the onset of photoemission at 0 eV binding energy was consistent with a metallic surface.

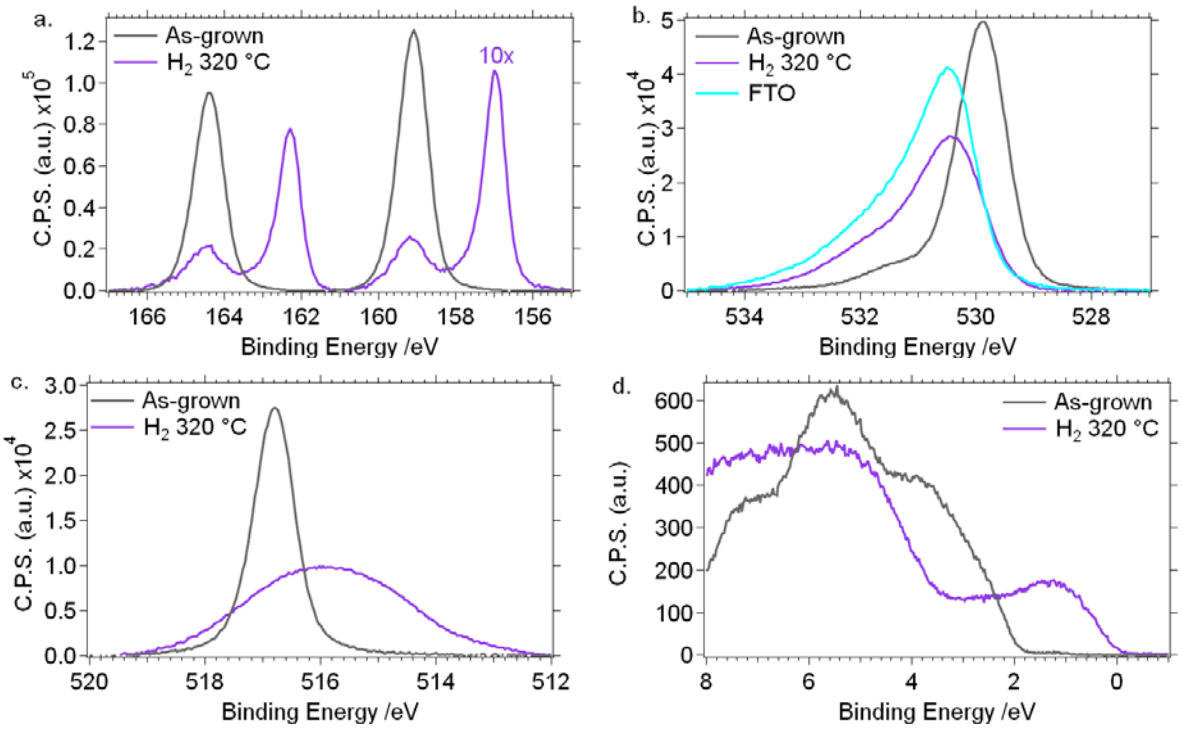

Figure S6. XPS spectra of $BiVO_4$/FTO annealed in H_2 at 320 °C (purple) and as-grown (black) for comparison, showing (a) Bi 4f, (b) O 1s, (c) V 3d, and (d) valence band energy ranges. The oxygen signal remaining after H_2-annealing at 320°C is due almost entirely to the substrate FTO, which has the O 1s spectrum shown in blue.

7. Density functional theory calculations of interstitial hydrogen

The density of states (DOS) of interstitial hydrogen (H_{int}) was calculated in the same manner as described in the main text for defect states. Here, neutral atomic hydrogen (H·) was added to the lattice and, after geometry optimization of the H_{int} position bonded to oxygen, the DOS shows H 1s DOS within both the

valence and conduction band of the $BiVO_4$ (Figure S7). The Fermi level was found to lie within the conduction band.

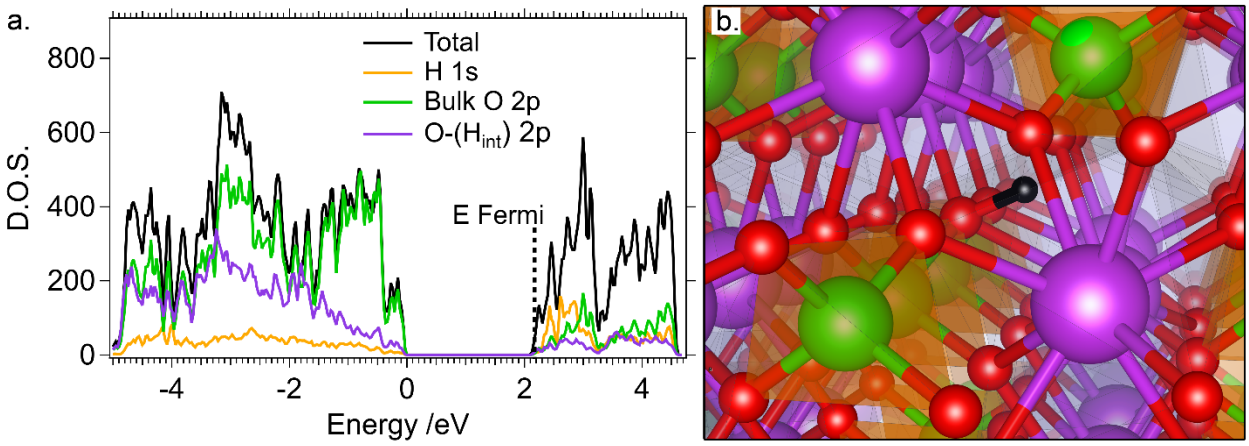

Figure S7. (a) Density of states (DOS) of interstitial hydrogen (H_{int}) in monoclinic scheelite $BiVO_4$ showing the total, hydrogen 1s, bulk oxygen 2p, the oxygen 2p states from the oxygen bound to hydrogen. (b) A geometry optimized interstitial hydrogen position in the $BiVO_4$ lattice.

8. Photoluminescence spectroscopy

The photoluminescence spectra, collected as intensity versus wavelength, were converted to photon flux versus photon energy using Equation S1; this is especially important prior to analysis and fitting of such broad features.

$$I_0(\lambda)d\lambda = I_0[\lambda(E)]dE\frac{d\lambda}{dE} = I_0[\lambda(E)]\frac{\lambda^2}{hc}(-dE) = \frac{\lambda^2 I_0}{1240\ eV\ nm}dE \qquad (S1)$$

Spectral fitting revealed two components, centered at 1.86 and 1.6 eV, and dominated by the peak at 1.86 eV (Figure S8). As a function of temperature, up to room temperature, the relative ratio between these two peaks remained approximately constant.

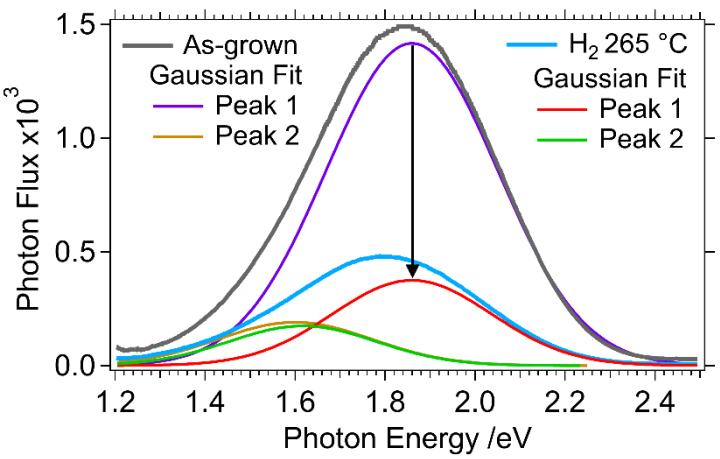

Figure S8. Gaussian fitting of photoluminescence spectra from spin-coated $BiVO_4$ thin films on quartz glass substrates: as-grown (grey) and after H_2 annealing at 265 °C (blue).

The temperature dependence of the integrated photoluminescence intensity, collected in the range of 11 K to 350 K, is shown for both thin film and powder samples (Figure S9). The thermal quenching is governed by a two activated process, one at low temperature (<50 K) and another at high temperature (>50 K), with dominant quenching from the high temperature process. The PL quenching curves were well described with a two component Arrhenius relation, given by Equation S2:

$$I(T) = \frac{I_0}{1 + \alpha_1 \exp(-E_{T_1}/kT) + \alpha_2 \exp(-E_{T_2}/kT)} \qquad (S2).$$

Least squares fitting resulted in values of α_1 and α_2 of 4.07 and 3745, respectively; and values of E_{T_1} and E_{T_2} of 13 ± 1 meV and 68 ± 5 meV. The activation energies decrease slightly as a result of hydrogen annealing, to ~10 meV and ~60 meV. The fitting parameters are shown in Table S1, and the data and fits for the thin films and powders are shown in Figure S9b&d.

The presence of a very low activation energy can also arise due to thermalization of charge carriers from a shallow level. A low thermal activation barrier of E_{T_1} with a corresponding low value of α_1 is reminiscent of CdTe and other II-VI semiconductors in which an alternative DAP recombination model was proposed by Krustok *et al.*[1] to describe the low temperature quenching region. Here the low temperature decrease in PL intensity is attributed to the T^{-2} dependence on the capture cross section of the luminescent defect center. This model is presented in Equation S3, in which E_D is the activation energy of the donor:

$$I(T) = \frac{I_0}{1 + \phi_1 T^{3/2} + \phi_2 T^{3/2} \exp(-E_D/kT)} \qquad (S3).$$

We also find very good agreement with our data, in which E_D is 40 ± 2 meV. After H_2 annealing at 250, 265, and 290 °C the thermal deactivation barrier was reduced to 35 ± 2, 34 ± 3 meV, 32 ± 2 meV. A summary of the fit parameters for both models are presented in SI Table S2 and figures showing the fits for thin films and powders are shown in SI Figure S9a&c.

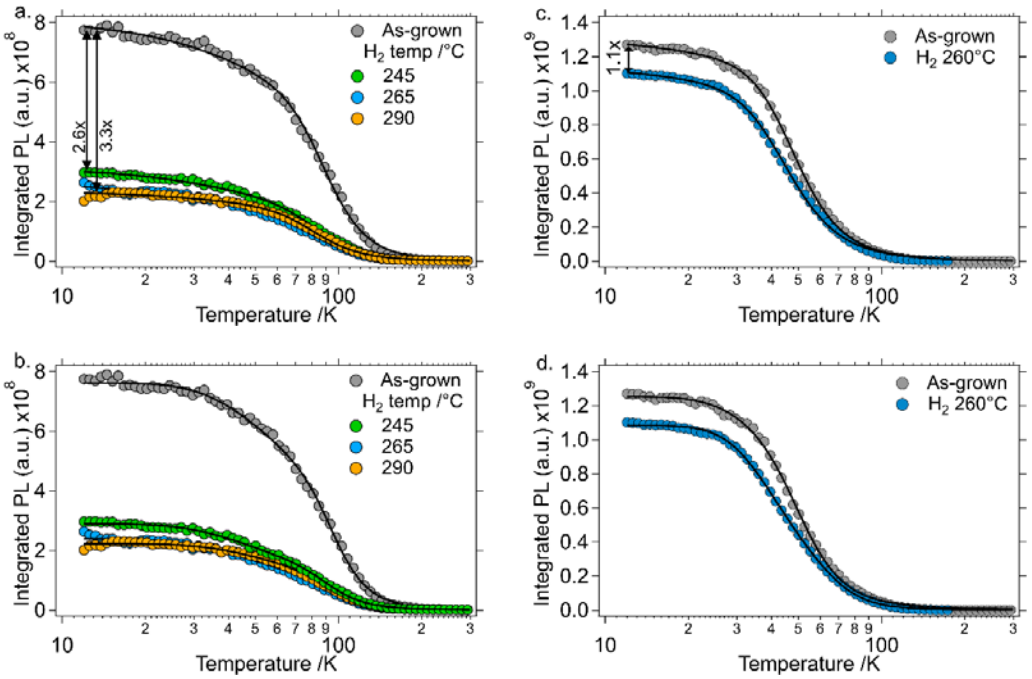

Figure S9. Integrated photoluminescence intensity as a function of temperature measured from as-grown and hydrogen-annealed $BiVO_4$ thin films spin-coated on quartz (a&b) and powder $BiVO_4$ samples (c&d). (a&c) Krustok fitting (solid traces) calculated with Equation S3, with fit coefficients reported in Table S2. (b&d) Arrhenius fitting (solid traces) calculated with Equation S2 and fit coefficients reported in Table S1.

Table S1. Fitting parameters determined from the least squares analysis of Equation S2 (double Arrhenius model) to model the temperature dependence of the integrated photoluminescence intensity.

Sample	α_1	E_1 (meV)	α_2	E_2 (meV)
		Thin Films		
As-grown	3.6±0.5	11.9±0.7	3300±1000	66±3
H_2 245°C	4.3±0.5	10.4± 0.5	2210±800	59±3
H_2 265°C	4.2±0.7	9.6±0.7	1865±960	56±5
H_2 290°C	4.1±0.6	11.5±0.6	1800±600	59±3
		Powders		
As-grown	7±2	11±1	700±100	30±1
H_2 260	37±3	14.3±0.2	6200±2000	48±2

Table S2. Fitting parameters determined from the least squares analysis of Equation S3 (Krustok model) to model the temperature dependence of the integrated photoluminescence intensity.

Sample	ϕ_1	ϕ_2	E_D (meV)
	Thin Films		
As-grown	$8.2\text{x}10^{-4} \pm 4\text{x}10^{-5}$	0.22 ± 0.05	41 ± 2
H_2 245°C	$1.28\text{x}10^{-3} \pm 5\text{x}10^{-5}$	0.15 ± 0.04	35 ± 2
H_2 265°C	$1.53\text{x}10^{-3} \pm 8\text{x}10^{-5}$	0.16 ± 0.05	34 ± 3
H_2 290°C	$7.5\text{x}10^{-4} \pm 7\text{x}10^{-5}$	0.11 ± 0.03	32 ± 2
	Powders		
As-grown	$7.8\text{x}10^{-4} \pm 5\text{x}10^{-5}$	0.16 ± 0.01	17.4 ± 0.4
H_2 260°C	$9\text{x}10^{-4} \pm 1\text{x}10^{-4}$	0.11 ± 0.01	14.5 ± 0.5

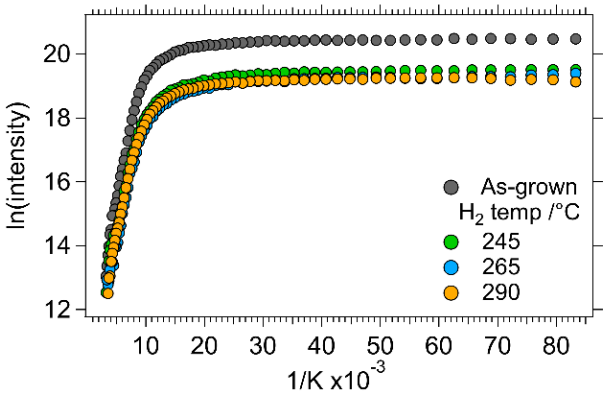

Figure S10. Arrhenius plot of the integrated photoluminescence intensity of $BiVO_4$ thin film samples as a function of temperature for the as-grown and various post-synthetic H_2-annealing treatments.

9. Temperature-dependent optical absorption

To determine whether the observed photoluminescence (PL) channels involved a band edge or could be ascribed to a DAP recombination channel, we measured the optical band gap as a function of temperature by optical adsorption spectroscopy. An untreated $BiVO_4$ thin film grown on quartz was studied from 10 K to 350 K. The band gap was calculated for each temperature by extrapolation of the Tauc plot adsorption onset to the background level. The Tauc plots as a function of temperature are shown in Figure S11a and the band gap is shown as a function of temperature in Figure S11b.

The bandgap of a semiconductor is expected to blue shift at low temperature due to a reduction of phonon broadening, as described by Equation S4, where $E_g(0)$ is the zero temperature bandgap energy, $\langle\hbar\omega\rangle$ is the average phonon energy, and S is a coupling constant:[2]

$$E_g(T) = E_g(0) - S\langle\hbar\omega\rangle[\coth(\langle\hbar\omega\rangle/2kT) - 1] \qquad \text{(S4)}.$$

The fit parameters are given in Figure S11b.

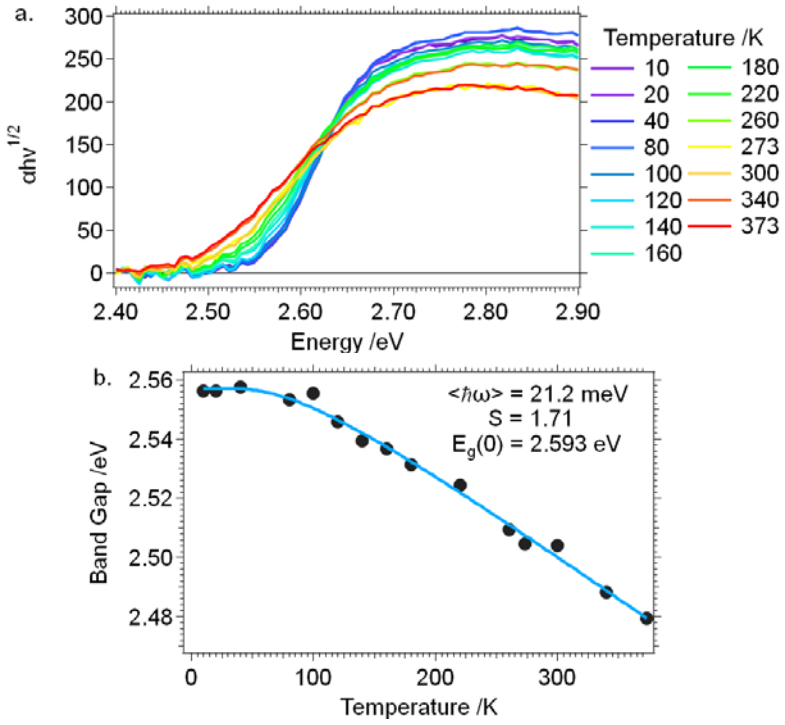

Figure S11. (a) Temperature-dependent Tauc plot of as-grown spin-coated $BiVO_4$ on quartz glass. (b) Band gap, determined from linear fitting of the absorption edge shown in (a), as a function of temperature (black dots). The fit using Equation S4 is shown as solid blue line, with fitting parameters also given.

References

1. J. Krustok, H. Collan and K. Hjelt, *Journal of Applied Physics*, 1997, **81**, 1442-1445.
2. K. P. O'Donnell and X. Chen, *Applied Physics Letters*, 1991, **58**, 2924-2926.